Physics Letters A 383 (2019) 1845–1849

Contents lists available at ScienceDirect

Physics Letters A

www.elsevier.com/locate/pla

Quantum communication through chains with diluted disorder

P.R.S. Júnior, G.M.A. Almeida, M.L. Lyra, F.A.B.F. de Moura *

Instituto de Física, Universidade Federal de Alagoas, Maceió, AL 57072-970, Brazil

ARTICLE INFO

Article history:
Received 30 August 2018
Received in revised form 8 March 2019
Accepted 10 March 2019
Available online 15 March 2019
Communicated by R. Wu

Keywords:
Quantum-state transfer
Anderson localization
Quantum communication

ABSTRACT

We investigate a single-qubit state transfer protocol along a channel featuring diagonal diluted disorder. In the regime where the source and destination sites are weakly coupled to the channel, we report the possibility of transmitting quantum states with high fidelity as well as establishing end-to-end entanglement in that sort of configuration. We further discuss how the performance of the protocol depends upon the availability of extended states within the disordered channel.

1. Introduction

The primary effect of disorder in quantum chains is to induce the so-called phenomenon of Anderson localization which suppresses propagation of the wave function. Based on the Anderson's early works [1] we know that the eigenstates of a single-particle tight-binding Hamiltonian with on-site uncorrelated disorder are exponentially localized for any degree of disorder in 1D systems. On the other hand, it was shown that the presence of correlations within the disorder distribution allows for the appearance of delocalized states in the band [2–16].

A particular class of correlated disorder put forward by Hilke in Ref. [9] consists of an Anderson model on which diagonal disorder is distributed throughout the lattice following a given periodicity. This *diluted* disorder model has been investigated in various frameworks since then [9–16]. The standard version of the model is based on two interpenetrating sub-lattices, one with random on-site potentials and the other featuring non-random segments of constant potentials. Special resonant energies emerge due to the periodicity of those segments. The diluted Anderson model was later modified to include a general diluting function which defines the on-site energies within each non-random segment [11]. Using an analytical procedure, it was demonstrated that this model displays a set of extended states, the number of which strongly depends on the length of the diluting segments and the symmetry of the function generating it. In Ref. [14] the electronic dynamics in diluted random chains was investigated in detail. The authors demonstrated that the wave function spreading profile strongly depends upon the initial position of the particle. Hilke [15] further investigated the diluted Anderson model in a square lattice, where a true metal-insulator transition with mobility edges delimiting a band of extended states was found.

Recently, correlated disorder has also been addressed in the context of quantum communication protocols. As it promotes the breakdown of Anderson localization, the coexistence between localized and extended states allows for the realization of quantum-state transfer (QST) [17] and entanglement distribution protocols [18] even in the presence of disorder. In reality, one should always expect the presence of some amount of disorder in pre-engineered quantum chains for QST protocols [17–26] due to experimental imperfections in the manufacturing process or dynamical factors. With this in mind, it is crucial to investigate the effects correlated noise on those protocols [17–20]. Such correlations offer the possibility of masking disorder without the need of substantial resources that would be required in order to globally diminishing it.

Here, we study a class of Rabi-type QST protocol where both ends of the chain are weakly coupled to the bulk [27–30], this featuring diluted disorder. By means of numerical diagonalization of the full Hamiltonian of the system we evaluate the QST input-averaged fidelity [31] as well as the end-to-end entanglement over a fixed time window. Our calculations reveal an interesting dependence of those quantities upon the resonances that exist within the channel due to the diluted disorder. We discuss those results in light of the existence of extended states in the set of normal modes of the channel.

2. Model

We consider a 1D spin chain (XX type) with $N+2$ sites described by the following Hamiltonian ($\hbar = 1$)

* Corresponding author.
E-mail address: fidelis@fis.ufal.br (F.A.B.F. de Moura).

https://doi.org/10.1016/j.physleta.2019.03.010
0375-9601/

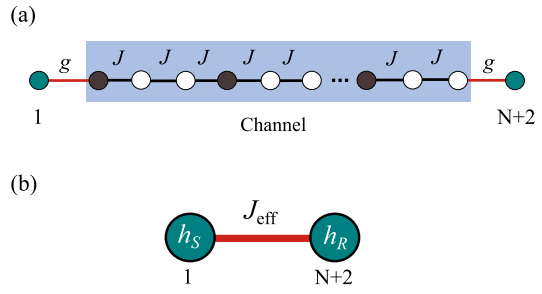

Fig. 1. (a) Model scheme: both outer spins, the communicating parties, are weakly coupled to the channel, that is $g \ll J$, which is made by independent segments of one disordered site (dark circles) having its energy randomly picked out of the box distribution $[-0.5J, 0.5J]$ plus two clean ones featuring fixed energy ϵ_0. The intrachannel coupling J is set uniformly across the channel. (b) Effective end-to-end interaction derived from second-order perturbation theory. Both outer parties acquire renormalized local energies h_S and h_R and create their own subspace, becoming connected via $J_{\rm eff}$ that depends on the spectral resolution of the channel. The working mechanism of the protocol is to make use of such reduced two-site configuration to induce Rabi-like oscillations between the outer spins.

$$H = W\left(|1\rangle\langle 1| + |N+2\rangle\langle N+2|\right) + \sum_{j=2}^{N+1} \epsilon_j |j\rangle\langle j| + J\sum_{j=2}^{N} |j\rangle\langle j+1| + g\left(|1\rangle\langle 2| + |N+1\rangle\langle N+2|\right) + \text{H.c.}, \tag{1}$$

with the first and last sites denoting the source and receiver components, respectively, having local energy $\epsilon_1 = \epsilon_{N+2} = W$ and coupled to the channel (made up by sites 2 through $N+1$) both at rate g. Here, state $|i\rangle \equiv |\downarrow\rangle_1 |\downarrow\rangle_2 \cdots |\uparrow\rangle_i \cdots |\downarrow\rangle_{N+2}$ denotes a single spin up at the $i-$th site. We set the hopping strengths in the channel as the energy unit, i.e., $J \equiv 1$. The diluted random on-site energies ϵ_j in the channel is generated in the following manner. For $j = 2, 5, 8, 11, \ldots$, ϵ_j are random numbers taken uniformly from the interval $[-0.5J, 0.5J]$ whereas for $j = 3, 4, 6, 7, 9, 10, 12, 13, \ldots$ we have a pure sub-lattice with energies given by $\epsilon_j = \epsilon_0$. According to this construction rule, one out of each three sites has a random local energy [see Fig. 1(a)]. In order to maintain the periodicity of these segments, which is the very ingredient responsible for inducing a set of delocalized states within the spectrum [11,13], here we fix the number of sites of the channel, N, to be a multiple of three. We also restrict ourselves to the weak coupling regime $g \ll J$. In this configuration, QST is performed via Rabi-like oscillations due to an effective interaction between the outer ends of the chain [27,28,30].

3. Quantum-state transfer protocol

In order to transmit an arbitrary qubit state $|\phi\rangle = a|\uparrow\rangle + b|\downarrow\rangle$ using the natural dynamics of the Hamiltonian defined above, we follow the standard QST scheme put forward by Bose in Ref. [31]. When initializing the channel and receiver at their ground state, the full initial state reads $|\psi(0)\rangle = |\phi\rangle_1 |\downarrow\rangle_2 \cdots |\downarrow\rangle_{N+2}$. Given that the underlying Hamiltonian of the system preserves the number of excitations, the actual dynamics here takes place in the single-excitation manifold and can thus be generated by a Hamiltonian having the form of Eq. (1). We then let the system evolve through e^{-iHt} until state $|\phi\rangle$ is available at site $N+2$ with highest possible fidelity $F_\phi(\tau) = \langle\phi|\rho_{N+2}|\phi\rangle$ – at some (prescribed) time τ – where ρ_{N+2} is the reduced state of the system after tracing out sites 1 through $N+1$. An appropriate figure of merit for the transfer is obtained by averaging F_ϕ over every possible input (that is over the Bloch sphere) to obtain [31]

$$F(t) = \frac{1}{2} + \frac{|f_{N+2}(t)|}{3}\cos\varphi + \frac{|f_{N+2}(t)|^2}{6} \tag{2}$$

where $f_{N+2}(t) = \langle N+2|e^{-iHt}|1\rangle$ represent the end-to-end transition amplitude and φ is its phase which can be generally neglected (we set $\cos\varphi = 1$ henceforth) by a suitable choice of the external potentials after the protocol is done.

We can work out that transition amplitude in the weak-coupling regime $g \ll J$ using second-order perturbation theory for Hamiltonian (1) [28]. Given $|\lambda_k\rangle = \sum_{j=2}^{N+1} v_{k,j}|j\rangle$ and λ_k are, respectively, the eigenstates and eigenvalues of the *channel* Hamiltonian $H_{\rm ch} \equiv \sum_{j=2}^{N+1} \epsilon_j |j\rangle\langle j| + J(\sum_{j=2}^{N} |j\rangle\langle j+1| + \text{H.c.})$, we may rewrite Eq. (1) as

$$H = W\left(|1\rangle\langle 1| + |N+2\rangle\langle N+2|\right) + \sum_k \lambda_k |\lambda_k\rangle\langle\lambda_k| + g\sum_k \left(v_{k,2}|1\rangle\langle\lambda_k| + v_{k,N+1}|N+2\rangle\langle\lambda_k| + \text{H.c.}\right). \tag{3}$$

This picture tells us that deep in the limit $g \ll J$ the outer spins, each with on-site energy W, either get in narrow resonance with one or the channel modes, say $W = \lambda_{k'}$, or does not. The former situation leads to an effective three-level system whereas the latter, off-resonant case, promotes the appearance of a reduced two-level subspace [28] spanned by both communicating parties, which is the most likely outcome given we are dealing with a disordered channel (the energy spectrum fluctuates sample by sample). So, whenever $W \neq \lambda_k$ for all k we are able to derive the following two-site effective Hamiltonian [see Fig. 1(b)]

$$H_{\rm eff} = h_S|1\rangle\langle 1| + h_R|N+2\rangle\langle N+2| + J_{\rm eff}(|1\rangle\langle N+2| + \text{H.c.}) \tag{4}$$

with

$$h_S = W - g^2\sum_k \frac{|v_{k,2}|^2}{\lambda_k - W}, \tag{5}$$

$$h_R = W - g^2\sum_k \frac{|v_{k,N+1}|^2}{\lambda_k - W}, \tag{6}$$

$$J_{\rm eff} = -g^2\sum_k \frac{v_{k,2}v_{k,N+1}^*}{\lambda_k - W}. \tag{7}$$

Details on how to approach to these expressions can be seen in Ref. [28]. In principle, the above effective framework does not make any assumptions toward the topology of the channel; it could be any arbitrary network, disordered or not. Without going any further, it is immediate to see that the quality of the single-particle transfer from site 1 to $N+2$ (or backwards) should depend on the detuning $\Delta = h_S - h_R$. Indeed, after diagonalization of the effective Hamiltonian [Eq. (4)] we get

$$|\xi^{\pm}\rangle = \frac{2J_{\rm eff}|1\rangle + (\Delta \pm \Omega)|N+2\rangle}{\sqrt{(\Delta \pm \Omega)^2 + 4J_{\rm eff}^2}}, \tag{8}$$

where $\Omega = \sqrt{\Delta^2 + 4J_{\rm eff}^2}$ is the effective Rabi frequency. The corresponding energies read $\xi^{\pm} = (h_S + h_R \pm \Omega)/2$. The absolute value of the transition amplitude finally takes the form

$$|f_{N+2}(t)| = \left|\frac{2J_{\rm eff}}{\Omega}\sin\left(\frac{\Omega}{2}t\right)\right|. \tag{9}$$

Thereby, we see that in order to get maximum fidelity [see Eq. (2)], one needs $\Delta = 0$, yielding $\Omega = 2J_{\rm eff}$ and then $|f_{N+2}(t)| = 1$ at times $\tau = n\pi/2|J_{\rm eff}|$ $(n = 1, 3, 5, \ldots)$. This is readily met when the channel is mirror symmetric, meaning that $|v_{k,2}| = |v_{k,N+1}|$ for every k or when the spectrum features particle-hole symmetry

– such as that of a chain with even number of sites with arbitrary couplings J_i and uniform on-site energies [30] – for which $\lambda_k = -\lambda_{-k}$ and $|v_{k,j}| = |v_{-k,j}|$, trivially leading to $h_S = h_R = 0$ as long as W is tuned at the very center of the band. (Note that mirror symmetry naturally implies particle-hole symmetry.)

Here, as we have to deal with on-site disorder, $\Delta \neq 0$ thereby decreasing the QST quality due to asymmetries within the channel band. On the other hand, we may minimize such effects by finding proper delocalizedlike states somewhere in the spectrum and tuning W accordingly (note that the contribution to the sums in Eqs. (5)-(7) decays as $(\lambda_k - W)^{-1}$ and thus modes distant from W becomes less relevant), so as to *balance* the overlaps $|v_{k,2}|$ and $|v_{k,N+1}|$ as much as possible and thus $|\Delta/J_{\text{eff}}| \ll 1$ to get $\Omega \approx 2J_{\text{eff}}$ [see Eqs. (2) and (9)]. Of course, that would be useless in the case of uncorrelated disorder, where every eigenstate is localized in 1D and 2D. Our goal here is then to track down sets of delocalized states induced in the diluted disorder model by controlling the sender-receiver energy W in order to maximize the QST fidelity.

We also mention that although disorder will make it somewhat difficult to define the exact transfer time τ realization by realization [17], here we are ultimately looking after the prospect of generating an end-to-end Rabi-like dynamics through a disordered chain having the characteristics discussed in the previous section. It also deserves to notice the fact that the effective Hamiltonian in Eq. (4) is an approximation. When considering the full system [Eq. (1)] we expect some leakage from the $\{|1\rangle, |N+2\rangle\}$ subspace into the channel during the evolution [27], given $H \neq H_{\text{eff}} \oplus H_{\text{ch}}$.

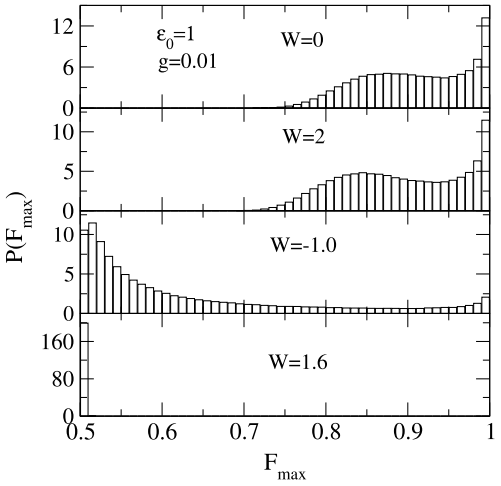

Fig. 2. Normalized probability distribution $P(F_{\max})$ versus $F_{\max} = \max\{F(t)\}$ evaluated over the time interval $tJ \in [0, 5 \times 10^5]$. Data were obtained from numerical diagonalization of Hamiltonian (1) for $N = 51$, $g = 0.01J$, $\epsilon_0 = 1J$, and 10^4 distinct disorder realizations.

4. Results

We start by showing our results for the maximum achieved fidelity $F_{\max} = \max\{F(t)\}$ over a fixed time interval $tJ \in [0, 5 \times 10^5]$ for many distinct disordered samples (Fig. 2). Calculations were done through exact numerical diagonalization of the full Hamiltonian [Eq. (1)]. In each histogram of Fig. 2 we considered different sender/receiver local frequencies W. We readily note that the fidelity is very sensitive against it. For $W = 0$ and $2J$, the majority of the samples fell around $F_{\max} \approx 1$ whereas $W = -1J$ resulted in a well spread distribution. The frequency $W = 1.6J$ had the poorest transfer quality ($F_{\max} \approx 1/2$).

In order learn more about this dependence of the fidelity over W, in Fig. 3 we show $F_{\max}$ averaged over distinct realizations within the same time interval as before, now for two different channel sizes. First, we note that there are two windows of W for which the transfer quality approaches unit and is weakly sensitive

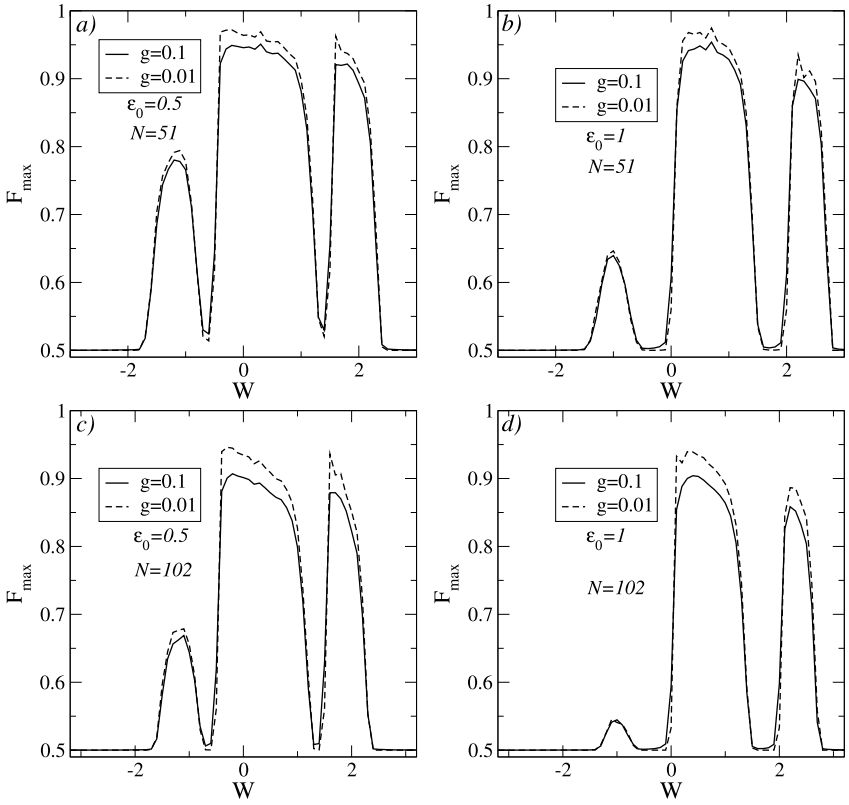

Fig. 3. Maximum fidelity $F_{\max}$ versus W (evaluated within $tJ \in [0, 5 \times 10^5]$) averaged over 10^3 independent realizations of disorder for $N = 51, 102$ and $\epsilon_0 = 0.5J, 1J$. Data were obtained from the exact numerical diagonalization of the Hamiltonian (1) with $g = 0.1J$ (solid lines) and $0.01J$ (dashed lines).

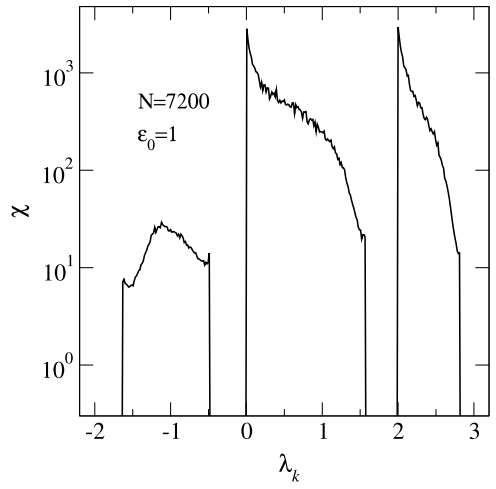

Fig. 4. Participation number χ versus channel eigenenergy λ_k for $N = 7200$ sites and $\epsilon_0 = 1J$ averaged over 10^3 disorder realizations. Note that the participation number becomes of the order of the chain size at energies 0 and $2J$, signaling the delocalized resonant states. Within the first band, χ reaches a maximum of the order of a few dozens of sites.

to the chain size. Moreover, we observe a third (less pronounced) window with high-fidelity centered at negative energies. This is not, however, a robust QST window for it is clearly associated to a finite-size effect, being visibly degraded for larger N. These aspects can be explained by analyzing the nature of the normal modes of the channel. Based on Ref. [13], chains with diluted disorder similar to the one we are using here feature two resonances within the band of allowed states. These resonances correspond to Bloch states with vanishing amplitude at the disordered sites. The Bloch states have eigenenergies given by $E_k = \epsilon_0 - 2J\cos k$, with $k = 2\pi/\zeta$ and ζ being the associated wavelength. In the present case, the resonant ones are $\zeta = 6$ and $\zeta = 3$ and thus for, say $\epsilon_0 = 1J$, the resonant energies are 0 and $2J$, around which it occurs the highest QST fidelity outcomes. In Ref. [13] it was further demonstrated that the Lyapunov exponent is finite for all energies except at those two values. We mention that although we are enforcing some sort of periodicity throughout the channel – for which the above properties hold – by only considering independent segments made up by a disordered site followed by two clean ones (see Fig. 1(a)), if we break it down at the end of the channel, say, by considering $N = 52$ or $N = 53$, the overall behavior would be about the same given we are dealing with small chains.

It is important to highlight that there is a finite region in the vicinity of the resonant energies in which the localization length is extremely pronounced (but finite). This is illustrated in Fig. 4 on which we plot the participation number, given by $\chi(\lambda_k) = (\sum_j |v_{k,j}|^4)^{-1}$, versus energy averaged over many disorder realizations for a chain with $N = 7200$ sites. Notice that the participation number remains quite large for energies above the resonances, thus supporting an efficient QST in the finite energy bands reported in Fig. 3. It also explains the loss of QST efficiency in the first band. When the chain size exceeds a few dozens of sites, it becomes much larger than the localization length in this low-energy band. Therefore, within the context of QST along a finite channel, only modes with large localization length contribute to the high fidelity of the transmission, effectively diminishing the ratio $|\Delta/J_{\text{eff}}|$ [see Eqs. (5) through (7)].

Back to Fig. 3, we also note that increasing N will lead to a fidelity decrease over the entire range of W. This is due to the allocation of more channel modes closer to W thereby disturbing the reduced subspace $\{|1\rangle, |N+2\rangle\}$. This can be solved by further lowering g at the expense of increasing the QST timescale given $\tau \sim g^{-2}$ [28,30].

Last, we investigate the creation of pairwise entanglement that occurs during the dynamics of the single-particle transfer from one end to the other. If one prepares $|\psi(0)\rangle = |1\rangle$, and arrange for $\Delta = h_S - h_R = 0$ in the effective model [Hamiltonian (4)], for instance, we get a fully entangled state of the form

$$|\psi(t')\rangle = \frac{|1\rangle + e^{i\varphi}|N+2\rangle}{\sqrt{2}} = \left(\frac{|\uparrow\rangle_1|\downarrow\rangle_{N+2} + e^{i\varphi}|\downarrow\rangle_1|\uparrow\rangle_{N+2}}{\sqrt{2}}\right) \otimes |\downarrow\rangle_{\text{channel}} \qquad (10)$$

at times $t' = \tau/2$.

We formally quantify the end-to-end entanglement by means of the so-called concurrence [32] which in our case (single-particle manifold) is simply [18]

$$C(t) = 2|f_1(t) f^*_{N+2}(t)| = \sqrt{|f_{N+2}(t)|^2 - |f_{N+2}(t)|^4}. \qquad (11)$$

Therefore, in the limit $g \ll J$ for which the effective Hamiltonian [Eq. (4)] is valid and the transition amplitude can be expressed as in Eq. (9), the concurrence reaches its maximum value $C = 1$ whenever the occupation probability of the particle to be in site $N+2$ is $p_{N+2} \equiv |f_{N+2}(t)|^2 = 1/2$. By examining Eq. (9) and recalling that $\Omega = \sqrt{\Delta^2 + 4J^2_{\text{eff}}}$, when $|\Delta/J_{\text{eff}}| < 2$ meaning $p^{(\max)}_{N+2} > 1/2$, the concurrence will always have two local maximum surrounding the p_{N+2} peak. When $|\Delta/J_{\text{eff}}| \geq 2$ ($p^{(\max)}_{N+2} \leq 1/2$), then both quantities reach about their maximum at the same time although the transmission (that is the fidelity) is already insignificant. On the other hand, entanglement remains strong up to $|\Delta/J_{\text{eff}}| = 2$, above which the maximum concurrence starts to decrease from $C = 1$.

Getting back to the full Hamiltonian [Eq. (1)] featuring small, but finite g, we now evaluate in the maximum concurrence $C_{\max} = \max\{C(t)\}$ achieved over the same time interval as in Fig. 3 and plot it against W in Fig. 5. As we expect from the discussion carried out above, the concurrence is indeed much more reliable against disorder (compare it with Fig. 3). It is worth stressing that in Fig. 5 we have considered the same parameters as in Fig. 3 when investigating the maximum fidelity. Needless to say, the resonance properties of the channel discussed at the beginning of this section applies here as well.

5. Summary and conclusions

In summary, we investigated QST and entanglement generation protocols over a 1D chain with weak end couplings featuring a particular kind of noise named diluted disorder, where the random on-site energies are set following a given periodicity. We showed that the existence of special resonances within the energy band of the channel allows for a high-quality realization of the above quantum information tasks even in the presence of disorder.

The overall performance of the channel primarily depends upon inducing an effective, reduced interaction between the outer ends of the chain (setting $g \ll J$) and making sure that there is a proper set of delocalized states around the tuning frequency W, that ultimately yields $|\Delta/J_{\text{eff}}| \ll 1$ for the QST protocol or, at least $|\Delta/J_{\text{eff}}| \leq 2$ for the entanglement generation procedure. In such diluted disorder model, the fidelity of the protocols is enhanced whenever W matches Bloch-like resonant modes with vanishing amplitude at the disordered sites. It is important to stress that the location of those resonant modes can be tuned by properly tailoring the energy profile in the non-random segments, thus opening the possibility of carrying out efficient quantum communication schemes for any specific frequency associated with the sender and receiver sites.

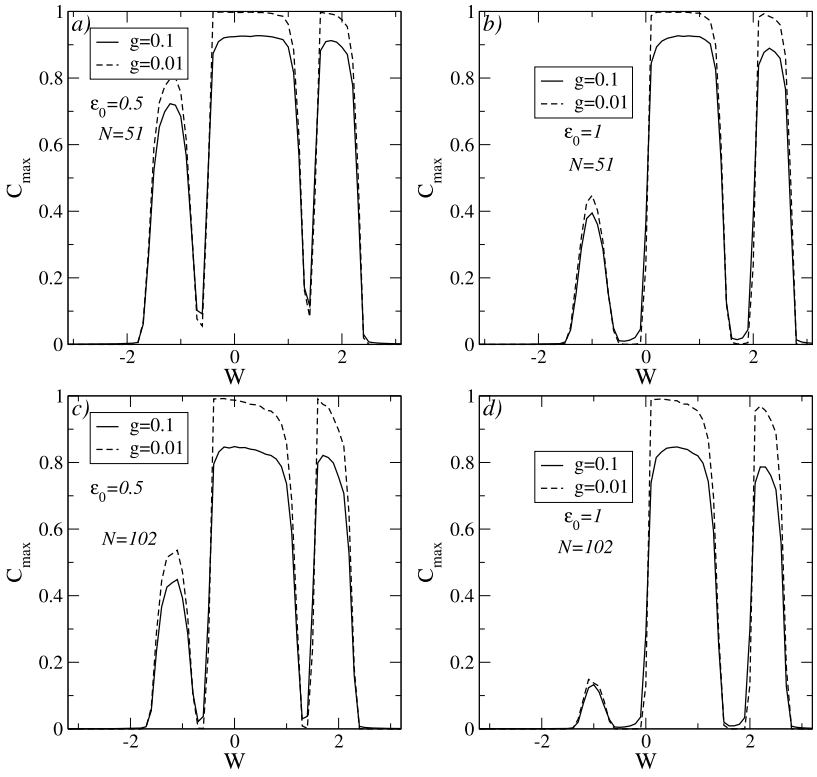

Fig. 5. Maximum concurrence $C_{\max}$ versus W (evaluated within $tJ \in [0, 5 \times 10^5]$) averaged over 10^3 independent realizations of disorder for $N = 51, 102$ and $\epsilon_0 = 0.5J, 1J$. Data were obtained from exact numerical diagonalization of the Hamiltonian (1) with $g = 0.1J$ (solid lines) and $0.01J$ (dashed lines).

Acknowledgements

This work was partially supported by the Brazilian research agencies CNPq and CAPES, as well as by the Alagoas state research agency FAPEAL.

References

[1] E. Abrahams, P.W. Anderson, D.C. Licciardello, T.V. Ramakrishnan, Phys. Rev. Lett. 42 (1979) 673.
[2] J.C. Flores, J. Phys. Condens. Matter 1 (1989) 8471.
[3] D.H. Dunlap, H.-L. Wu, P.W. Phillips, Phys. Rev. Lett. 65 (1990) 88;
H.-L. Wu, P. Phillips, Phys. Rev. Lett. 66 (1991) 1366;
P.W. Phillips, H.-L. Wu, Science 252 (1991) 1805.
[4] S. Gangopadhyay, A.K. Sen, J. Phys. Condens. Matter 4 (1992) 3725.
[5] P.K. Datta, D. Giri, K. Kundu, Phys. Rev. B 47 (1993) 10727.
[6] S.N. Evangelou, D.E. Katsanos, Phys. Lett. A 164 (1992) 456.
[7] F.M. Izrailev, A.A. Krokhin, N.M. Makarov, Phys. Rep. 512 (2012) 125.
[8] F.A.B.F. de Moura, M.L. Lyra, Phys. Rev. Lett. 81 (1998) 3735.
[9] M. Hilke, J. Phys. A 30 (1997) L367.
[10] F. Domínguez-Adame, I. Gomez, A. Avakyan, D. Sedrakyan, A. Sedrakyan, Phys. Status Solidi B 221 (2000) 633.
[11] E. Lazo, M.E. Onell, Physica B 299 (2000) 173;
E. Lazo, M.E. Onell, Phys. Lett. A 283 (2001) 376.
[12] S.S. Albuquerque, F.A.B.F. de Moura, M.L. Lyra, Physica A 266 (2005) 465.
[13] F.A.B.F. de Moura, M.N.B. dos Santos, U.L. Fulco, E. Lazo, M. Onell, M.L. Lyra, Eur. Phys. J. B 36 (2003) 81.
[14] S.S. Albuquerque, F.A.B.F. de Moura, M.L. Lyra, E. Lazo, Phys. Lett. A 355 (2006) 468.
[15] M. Hilke, Phys. Rev. Lett. 91 (2003) 226403.
[16] A.E.B. Costa, F.A.B.F. de Moura, Eur. Phys. J. B 80 (2011) 59.
[17] G.M.A. Almeida, F.A.B.F. de Moura, M.L. Lyra, Phys. Lett. A 382 (2018) 1335.
[18] G.M.A. Almeida, F.A.B.F. de Moura, T.J.G. Apollaro, M.L. Lyra, Phys. Rev. A 96 (2017) 032315.
[19] G. De Chiara, D. Rossini, S. Montangero, R. Fazio, Phys. Rev. A 72 (2005) 012323.
[20] D. Burgarth, S. Bose, New J. Phys. 7 (2005) 135.
[21] D.I. Tsomokos, M.J. Hartmann, S.F. Huelga, M.B. Plenio, New J. Phys. 9 (2007) 79.
[22] N.Y. Yao, L. Jiang, A.V. Gorshkov, Z.-X. Gong, A. Zhai, L.-M. Duan, M.D. Lukin, Phys. Rev. Lett. 106 (2011) 040505.
[23] A. Zwick, G.A. Álvarez, J. Stolze, O. Osenda, Phys. Rev. A 84 (2011) 022311.
[24] S. Lorenzo, T.J.G. Apollaro, A. Sindona, F. Plastina, Phys. Rev. A 87 (2013) 042313.
[25] S. Ashhab, Phys. Rev. A 92 (2015) 062305.
[26] M.P. Estarellas, I. D'Amico, T.P. Spiller, Phys. Rev. A 95 (2017) 042335.
[27] A. Wójcik, T. Łuczak, P. Kurzyński, A. Grudka, T. Gdala, M. Bednarska, Phys. Rev. A 72 (2005) 034303.
[28] A. Wójcik, T. Łuczak, P. Kurzyński, A. Grudka, T. Gdala, M. Bednarska, Phys. Rev. A 75 (2007) 022330.
[29] G.M.A. Almeida, F. Ciccarello, T.J.G. Apollaro, A.M.C. Souza, Phys. Rev. A 93 (2016) 032310.
[30] G.M.A. Almeida, Phys. Rev. A 98 (2018) 012334.
[31] S. Bose, Phys. Rev. Lett. 91 (2003) 207901.
[32] W.K. Wootters, Phys. Rev. Lett. 80 (1998) 2245.